Temperature-dependent renormalization of magnetic interactions by thermal, magnetic, and lattice disorder from first principles

Matthew Heine [1], Olle Hellman [2], and David Broido[1,*]

[1]*Department of Physics, Boston College, Chestnut Hill, Massachusetts 02467, USA*
[2]*Department of Physics, Chemistry and Biology (IFM), Linköping University, SE-581 83 Linköping, Sweden*

We put forth an *ab initio* framework to calculate local moment magnetic interaction parameters, renormalized to treat both the lattice and magnetic systems as a function of temperature T. For bcc Fe, magnetic and lattice thermal disorders act in opposition, the former strengthening the Heisenberg-like interactions, while the latter decreasing them. Below T_C, J stays nearly independent of T, while around and above T_C, it exhibits a sharp decrease. This remarkable behavior reflects an intricate spin-lattice coupling and its evolution with T, in which magnetic interactions and interatomic bonds are each renormalized by the other. This finding is consistent with magnetization data and with the observed softening of magnon and phonon modes at high temperatures. Magnetization as well as magnon and phonon mode softening are discussed.

I. INTRODUCTION

The temperature dependence of magnetism has long been a challenge for first-principles calculations. Of particular importance are magnetic systems described by Heisenberg, Kitaev, and Dyaloshinski-Moriya (DM) interactions. Many theories approximate the magnetic interaction strengths using temperature-independent constants [1–8]. With increasing temperature, quasiparticle excitations such as magnons and phonons are renormalized by the growing thermal disorder in magnetic and lattice subsystems and by the mutual coupling of these subsystems. Yet, the impact of temperature on magnetic interaction strengths has received little attention.

Perhaps the most studied case is that of iron [5–25]. Early attempts in Fe focused on including the finite temperature of the magnetic system, while neglecting that of the lattice [6,12,20–25]. The lattice and magnetic degrees of freedom in iron are intimately coupled [9,11,14], and recent calculations [15] found thermal lattice disorder, i.e., the temperature-dependent displacements of atoms about their equilibrium positions, to have a significant impact on the magnetism at the Curie temperature T_C.

This raises many interesting questions. First, the calculations in Ref. [15] were performed at a single temperature, near T_C. Do the same conclusions about the importance of thermal lattice disorder also hold for other temperatures? What is the evolution of the magnetic interaction strength with temperature? Prior calculations where lattice atoms were fixed to their classical equilibrium positions [25] found an increase of first-nearest-neighbor magnetic interaction strength with increasing temperature; given the results of Ref. [15], might this trend simply be an artifact of the use of an ideal (nonthermal) lattice in the former work?

Moreover, the calculations of Ref. [15] neglected the effect of magnetic thermal disorder, i.e., the temperature-dependent rotation of moments away from ferromagnetic alignment, upon the lattice, even around $T_C = 1043$ K. However, the lattice dynamics in bcc Fe has been demonstrated [11,14] to be sensitive to thermal magnetic disorder; at temperatures near T_C, vibrational properties differ significantly from those of a ferromagnetic state. If the magnetic interaction is sensitive to lattice thermal disorder, what then would be the effect of including thermally relevant magnetic disorder as well? A calculation of magnetic exchange as a function of temperature including both realistic magnetic and lattice thermal disorder is lacking. Additionally, given the sensitivity of both systems, is there any evidence of higher-order spin-lattice coupling effects whereby thermal magnetic disorder may renormalize the magnetic interaction via renormalizing the lattice dynamics?

Perhaps the most common tool for investigating magnetism is a local-moment model $H = -\frac{1}{2} \sum_{i,j,\alpha,\beta} J_{i,j}^{\alpha,\beta} e_i^\alpha e_j^\beta$, where e_i^α is the αth Cartesian component of a unit vector representing the direction of the local magnetic moment at site i, and $J_{i,j}^{\alpha,\beta}$ is a magnetic exchange parameter which represents the strength of the magnetic interaction between the moments at sites i and j, and α and β are Cartesian directions. In this model, the lengths of the moments are fixed but their directions may vary. The general form of this model encompasses Heisenberg, Kitaev, and DM interactions. The use of a Heisenberg form for iron has been justified in the disordered local moments picture for itinerant electron systems [21,22]. A standard first-principles analysis typically calculates $J_{i,j}$ values via perturbations of an ideal $T = 0$ system but then uses those same values at high temperatures ($T \approx T_C$) to calculate magnetization curves and T_C [5,6]. In this paper, we investigate the effects of allowing $J_{i,j}$ to vary with temperature T, in addition to volume V, in order to capture finite-temperature effects. This nonperturbative approach obtains $J_{i,j}(V, T)$ magnetic interactions as well as interatomic interactions which are

renormalized by coupled thermal effects in both systems. We focus on the effect of thermal lattice disorder as well as *direct* and *indirect* effects of thermal disorder in magnetic moment orientations. By *indirect* effects, we mean the following: The presence of magnetic thermal disorder affects the bonding between Fe atoms, which then affects the thermal displacements of the Fe atoms, which, in turn, affect J values. We then refer to the change in J caused by this renormalization of the lattice thermal disorder as an *indirect* effect of the magnetic thermal disorder.

II. TEMPERATURE RENORMALIZED HEISENBERG INTERACTIONS

The temperature-dependent effective potential (TDEP) framework [26–29] has been demonstrated to capture well spin-lattice coupling effects on phonons at finite temperature [14]. Here, we use the TDEP framework to extract effective Heisenberg-like magnetic exchange parameters. To this end, we adopt a Hamiltonian form of Eq. (1),

$$H = U_0(V, T) + \sum_{i,\alpha} \frac{(p_i^\alpha)^2}{2M_i}$$
$$+ \frac{1}{2} \sum_{i,j,\alpha,\beta} \Phi_{i,j}^{\alpha,\beta}(V, T) u_i^\alpha u_j^\beta - \frac{1}{2} \sum_{i,j,\alpha,\beta} J_{i,j}^{\alpha,\beta}(V, T) e_i^\alpha e_j^\beta,$$

(1)

where u_i^α is the αth Cartesian component of the displacement from equilibrium of the atom at site i. $\Phi_{i,j}^{\alpha,\beta}(V, T)$ are effective interatomic force constants (IFCs) relating the motion of an atom at site i to that of an atom at site j. Analogously for the magnetic system, e_i^α is a unit vector which represents the direction of the magnetic moment at site i in the lattice. $J_{i,j}^{\alpha,\beta}(V, T)$ is then an effective generalized magnetic exchange tensor characterizing the magnetic interaction between the magnetic moments at site i and j. Imposing bcc symmetry, the magnetic interaction tensor becomes diagonal $J_{i,j}^{\alpha,\beta}(V, T) = J_{i,j}(V, T)\delta_{\alpha,\beta}$. Note that, in the TDEP scheme, the IFCs and Heisenberg-like exchange parameters depend *explicitly* on both V and T and are renormalized to include higher-order effects including anharmonicity and spin-lattice coupling.

Then $\Phi_{i,j}^{\alpha,\beta}(V, T)$ and $J_{i,j}(V, T)$ are calculated by sampling the potential energy surface in thermally relevant spin-lattice configurations in the canonical ensemble. We emphasize that, at elevated temperatures, *both* the lattice *and* the magnetic moments are in thermally relevant configurations which are far from the static equilibrium ferromagnetic ideal lattice configuration. This is to be contrasted with calculations which only slightly perturb the ferromagnetic ideal lattice ground state, or calculations which treat only one subsystem at finite temperature, leaving the other system in the ideal, ordered configuration [5,7].

Thermal sampling is achieved via a variation of the stochastic sampling technique in Ref. [14]. A 54-atom bcc Fe supercell is considered at each V-T. For a given set of $\Phi_{i,j}^{\alpha,\beta}(V, T)$, phonon modes are extracted from the Hamiltonian in Eq. (1) and then populated stochastically

according to quantum statistics [14]. This is repeated to produce 10–40 different thermal lattice configurations in which every atom is displaced from its classical equilibrium position. We note that this approach incorporates zero-point motion. Then, for a given set of $J_{i,j}(V, T)$, Markov chain Monte Carlo [30–32] simulations employing the Metropolis algorithm [33] are performed for the magnetic portion of Eq. (1). In this way, an ensemble of 100–400 thermal magnetic supercell configurations are produced. A crucial point is that the same finite temperature is used in thermal magnetic and lattice supercell generation ($T_{\text{Magnetic}} = T_{\text{Lattice}} \equiv T$). Then, thermal spin-lattice supercell configurations are produced by combining each thermal lattice configuration with ten different thermal magnetic configurations. For instance, a combination of 40 lattice configurations and ten magnetic configurations produces a total of 400 spin-lattice configurations, each with a unique magnetic configuration but sharing the same lattice configuration with nine other spin-lattice snapshots. This strategy of combination allows solving for $J_{i,j}(V, T)$ as discussed below. The above is repeated for every V-T point studied.

The energy and atomic forces are calculated for every spin-lattice configuration from first principles within the framework of density functional theory (DFT). Fully non-collinear magnetic calculations are performed in VASP with spin-orbit coupling and moments constrained to the directions in the thermal spin-lattice configuration [34–38]. We used the projector augmented-wave (PAW) method [39,40], and the parametrization of the generalized gradient approximation according to Perdew, Burke, and Ernzerhof [41] was taken to treat the exchange correlation. A k mesh of $3 \times 3 \times 3$ was used with a plane-wave cutoff of 350 eV.

For each V-T, a set of energy differences is generated by subtracting energies for each pair of spin-lattice configurations that share the same lattice configuration. In this way, the portion of the energy attributable *explicitly* to atomic displacements is eliminated. We then solve for the set of $J_{i,j}(V, T)$ which best reproduces this set of energy differences according to Eq. (1). We then solve for the $\Phi_{i,j}^{\alpha,\beta}(V, T)$ that best reproduce the set of all forces in all spin-lattice configurations for this V-T [14]. This entire process is iterated until self-consistency is achieved. As a test, the self-consistent loops were started with two different seed values of $J_{i,j}(V, T)$ and $\Phi_{i,j}^{\alpha,\beta}(V, T)$ and the same final answer was obtained. In this work, $V(T)$ is obtained by following a thermal expansion curve constructed by combining the measured thermal expansion [42] with the $T = 0$ energy minimum obtained from the DFT calculations as in Ref. [14]; details are given in the Supplemental Material [43]. We found the effect of thermal expansion to be negligible.

III. RESULTS

Figure 1 displays the first-nearest-neighbor magnetic interaction parameter $J_1(T)$ for three cases. The red curve shows the fully renormalized $J_1(T)$, i.e., it has been fully iterated to self-consistency and includes effects from both magnetic and lattice thermal disorder as well as higher-order spin-lattice coupling effects. For all points above $T = 300$ K, the second-nearest-neighbor $J_2(T)$ value was found to be negligible,
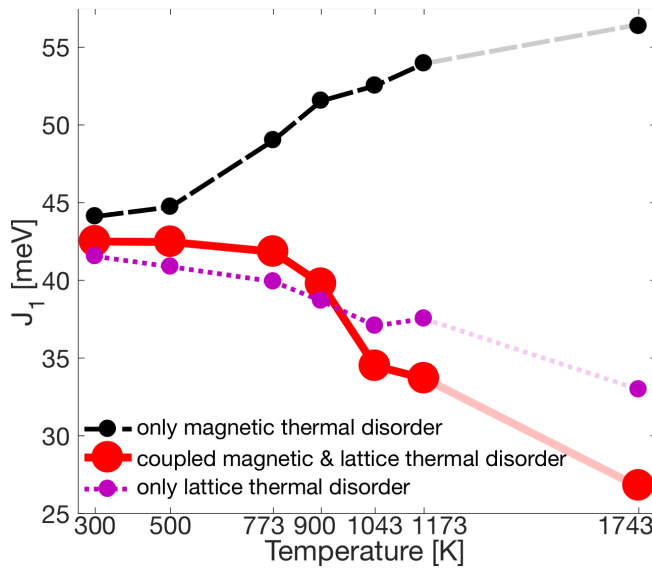
FIG. 1. Magnetic exchange parameter J_1 for Fe as a function of temperature for various degrees of inclusion of lattice and magnetic thermal disorder. Points are calculated values while lines are guides to the eye. The solid red curve includes realistic, self-consistent coupled thermal disorder in both the lattice and the magnetic systems. The black dashed curve includes only magnetic thermal disorder and no lattice thermal disorder. The purple dotted curve includes lattice thermal disorder but no magnetic thermal disorder. Curves are lightened between 1174 and 1743 K to signify that Fe is in a fcc phase between 1185 and 1667 K [44].
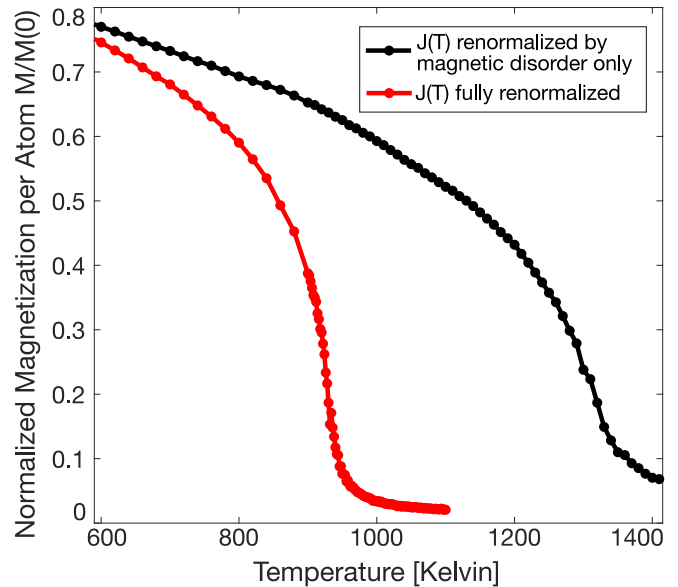

FIG. 2. Normalized magnetization per atom curves, $M(T)/M(0)$, for Fe calculated via Monte Carlo simulations. The red curve uses the full $J_1(T)$ (red curve from Fig. 1). The black curve uses the $J_1(T)$ which completely excludes lattice thermal disorder (black curve in Fig. 1). $M(0)$ is the magnetization per atom at $T = 0$ K. Curves are for 6750-atom simulations. Points are calculated values, and lines are guides to the eye.

consistent with the expectations of Ref. [25], so we consider only $J_1(T)$ here. Below about 900 K, the curve is flat, apparently justifying the commonly used temperature-independent model in that range. However, a central finding of this work is that the near-constant J_1 masks the fact that as T increases, the increasing magnetic and lattice thermal disorders drive J_1 in opposite directions, as shown below. Furthermore, the value of $J_1(T)$ decreases dramatically near T_C and continues to weaken as T is increased into the high-temperature δ phase of bcc Fe. Clearly the renormalization of J_1 is not uniform across all T, and so conclusions drawn near T_C may not readily apply for other T. We briefly examine some physical consequences of this temperature dependence before seeking its cause. For a given T, decreasing J_1 will result in increased magnetic disorder, as the ordering magnetic interactions between the moments is reduced. Therefore, as $T \rightarrow T_C$ from below, the rapid weakening of $J_1(T)$ causes magnetization $M(T)$ to fall to zero more rapidly near T_C than would be the case if J_1 were fixed at its low-T value. In the adiabatic limit, magnon dispersions may be connected quantitatively to the Heisenberg magnetic exchange parameters [6,45,46]. The validity of these relations near T_C is questionable, so we do not use this formulation to calculate magnon dispersions. However, it is reasonable to expect the magnon frequency scale to be set by the magnetic exchange strength even at elevated temperatures. Therefore, we may make a qualitative connection to the temperature dependence of magnon dispersions: The rapid drop in $J_1(T)$ near T_C implies that there should be a rapid decrease in magnon frequencies near T_C. This is in

qualitative agreement with experiment [47] which observed magnon frequencies to decrease more rapidly with increasing T in the range 918–1036 K than from 295 to 918 K.

But why does simultaneously incorporating the thermal disorder in lattice and magnetic systems give a nearly constant J_1 below T_C? And what drives its rapid decrease around T_C? We now endeavor to understand this interesting behavior and to isolate the effects of the lattice compared with those of the magnetic system.

First, we calculate the effect of thermal disorder in the magnetic system alone, while restricting the lattice atoms to reside at their equilibrium sites. This case is given by the black curve of Fig. 1, which indicates that increasing magnetic disorder on its own actually *increases* J_1, consistent with prior findings [25]. If, as previously discussed, magnon frequencies are assumed to follow $J_1(T)$, then this case of $J_1(T)$ renormalized only by magnetic thermal disorder is in qualitative disagreement with the experimentally observed sudden softening of magnon dispersions near T_C [47]. Consequences also exist for the corresponding magnetization curves, shown in Fig. 2. For a given T, thermal atomic motion decreases J_1 (Fig. 1), which necessarily decreases magnetization (Fig. 2), resulting in a T_C closer to the measured value of 1043 K than the case of including only magnetic thermal disorder.

At the opposite extreme, the purple curve in Fig. 1 includes lattice thermal disorder but suppresses magnetic thermal disorder. In the language introduced above, both *direct* and *indirect* effects of magnetic disorder are "turned off." Technical details of how this was achieved appear in the Supplemental

Material [43]. At 1043 K, both the red and purple curves in Fig. 1 lie significantly below the black curve, demonstrating that thermal lattice disorder strongly reduces the strength of the magnetic exchange at this temperature, in qualitative agreement with Ref. [15]. However, examining the full temperature range, we see a remarkable behavior. The temperature dependences of the black and purple curves are *opposite*, indicating that thermal lattice disorder and thermal magnetic disorder have competing effects on the magnetic exchange. As might be expected, these curves approach one another at low T, where thermal disorder in both systems lessens. Surprisingly, inclusion of only *lattice* thermal disorder proves to be a better approximation to the full calculation (comparing purple to red); this will be discussed further below.

Figure 1 also reveals that thermal lattice and magnetic disorders combine nonlinearly at elevated temperatures. For low and intermediate temperatures, $T = 300$–900 K, the full calculation (red) lies between the two extremes of only magnetic thermal disorder (black) and only lattice thermal disorder (purple). Thus, the near-constant J_1 for the full calculation below T_C is actually a result of canceling effects from the lattice and magnetic thermal disorder. Near and above T_C, however, the full calculation lies below *both* these extremes, indicating that magnetic and lattice thermal disorder combine nonlinearly in this region. This suggests that the observed softening of magnon frequencies at temperatures around T_C results from a nonlinear spin-lattice coupling. We turn our attention now to uncovering the nature of this nonlinearity.

To this end, we "turn off" the *direct* effects of magnetic thermal disorder but include *indirect* effects by restricting the magnetic thermal disorder to only influence J_1 through its renormalizing the lattice disorder [43]. The direct effect of magnetic disorder for T below 1043 K is to increase J_1 (i.e., shift up from blue to red curve), consistent with the black curve in Fig. 1. Therefore, one ingredient in the steep drop of the red curve near 1043 K is the direct effect of magnetic thermal disorder preventing a gradual drop below 1043 K.

For T at and above 1043 K, the behavior is quite different. Here, there is no *direct* effect of thermal magnetic disorder on $J_1(T)$, as the blue curve lies exactly on the red curve. Thus, the same values for $J_1(T = 1043$ K$)$ and $J_1(T = 1173$ K$)$ are obtained even when the proper magnetic configurations are swapped out for nearly ferromagnetic ones. This is a surprising result. What then directly drives the value of $J_1(T)$ in this region? If not the magnetic system, it must be the lattice. However, this seems an unusual proposition: T_C is a magnetic property, so why should the lattice induce a dramatic change near T_C? Does this mean that magnetic thermal disorder has no effect at and above $T = 1043$ K? We now turn to examining the direct effects of the lattice.

Previous calculations [11,14] have found a strong softening of phonon frequencies for temperatures near and above T_C, consistent with measurement [43,44,48]. Such behavior reflects a weakening of the interatomic bonds, driven by the transition from ferromagnetic toward paramagnetic magnetic moment orientations. This coupling between magnetic and atomic systems is therefore a mechanism by which the softening lattice could indirectly induce a significant reduction in $J_1(T)$, and consequently magnon frequencies, near and above T_C.
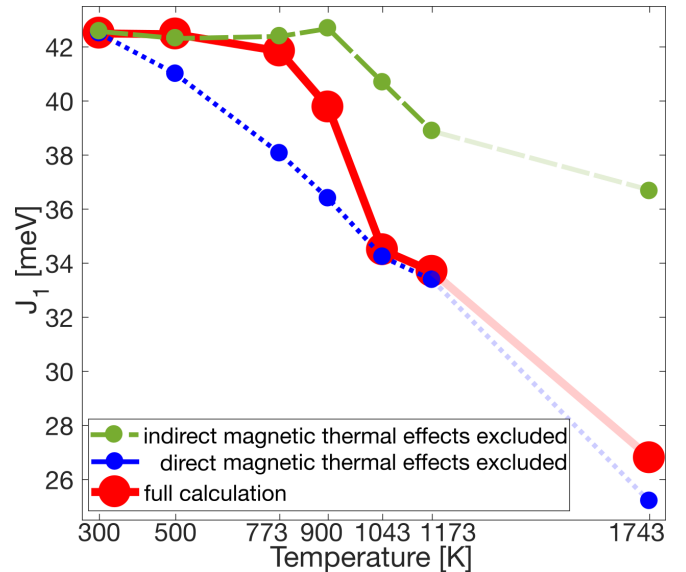

FIG. 3. Magnetic exchange parameter J_1 as a function of temperature with direct effects of magnetic thermal disorder artificially excluded (blue dotted) but indirect effects still present. Also the complementary case of direct effects included but indirect effects excluded (green dashed). The red curve is the full calculation (red curve from Fig. 1).

To investigate this possibility, we turn off the *indirect* effects of magnetic thermal disorder (green curve in Fig. 3). This case contrasts with the purple curve of Fig. 1, which omits both indirect and direct effects. Thus, the green curve represents the case where thermal magnetic disorder may affect $J_1(T)$ directly but is prevented from renormalizing the lattice thermal disorder. A comparison of the red and green curves in Fig. 3, shows that any *indirect* effects of magnetic thermal disorder on $J_1(T)$ are negligible for temperatures below 1043 K. However, indirect effects cause a significant suppression of $J_1(T)$ at and above 1043 K. We conclude that it is precisely this effect that induces the dramatic drop in $J_1(T)$ near T_C. It is a nonlinear, higher-order effect of spin-lattice coupling. All at once, the magnetic thermal disorder renormalizes the interatomic bonds thereby affecting the atomic thermal motion, which in turn renormalizes the magnetic interaction. Therefore, even though the magnetic thermal disorder does not *directly* affect $J_1(T)$ at and above 1043 K, it still affects it *indirectly*, with the lattice as an intermediary. The connection between $J_1(T)$ and magnon frequencies argued above implies that this nonlinear spin-lattice coupling effect drives a sudden softening of magnon modes with increasing T near T_C, in qualitative agreement with experiment. This is a higher-order spin-lattice effect than is included in previous theoretical treatments.

IV. SUMMARY AND CONCLUSIONS

In summary, we presented a computational scheme to calculate local-moment magnetic interaction parameters and interatomic force constants, including renormalization from thermal spin-lattice effects and applied it to bcc Fe. The temperature independence of magnetic interactions in iron is

revealed to arise from a competition between thermal disorder in the lattice and magnetic systems, which drive the magnetic interaction strength in opposite directions. Thus, inclusion of thermal disorder in both systems is necessary even to capture qualitative behavior. The sudden weakening of $J_1(T)$ near T_C is consistent with the measured softening of magnon modes in this region of temperatures. Here, we given a qualitative explanation of this observed behavior as resulting from a higher-order effect in which magnetic thermal disorder softens interatomic bonding which in turn weakens the magnetic interaction strength. This finding highlights the power of our theoretical framework, particularly the self-consistent coupled renormalization of the spin-lattice system.

[1] Y. Yamaji, Y. Nomura, M. Kurita, R. Arita, and M. Imada, Phys. Rev. Lett. **113**, 107201 (2014).

[2] Y. S. Hou, J. H. Yang, H. J. Xiang, and X. G. Gong, Phys. Rev. B **98**, 094401 (2018).

[3] T. Koretsune, T. Kikuchi, and R. Arita, J. Phys. Soc. Jpn. **87**, 041011 (2018) .

[4] M. Heide, G. Bihlmayer, and S. Blügel, Physica B: Condens. Matter **404**, 2678 (2009).

[5] A. Liechtenstein, M. Katsnelson, V. Antropov, and V. Gubanov, J. Magn. Magn. Mater. **67**, 65 (1987).

[6] S. V. Halilov, A. Y. Perlov, P. M. Oppeneer, and H. Eschrig, Europhys. Lett. **39**, 91 (1997).

[7] X. Tao, D. P. Landau, T. C. Schulthess, and G. M. Stocks, Phys. Rev. Lett. **95**, 087207 (2005).

[8] I. Turek, J. Kudrnovský, V. Drchal, P. Bruno, and S. Blügel, Phys. Status Solidi B **236**, 318 (2003) .

[9] Q. Han, T. Birol, and K. Haule, Phys. Rev. Lett. **120**, 187203 (2018).

[10] Y. O. Kvashnin, R. Cardias, A. Szilva, I. Di Marco, M. I. Katsnelson, A. I. Lichtenstein, L. Nordström, A. B. Klautau, and O. Eriksson, Phys. Rev. Lett. **116**, 217202 (2016).

[11] F. Körmann, B. Grabowski, B. Dutta, T. Hickel, L. Mauger, B. Fultz, and J. Neugebauer, Phys. Rev. Lett. **113**, 165503 (2014).

[12] A. Szilva, M. Costa, A. Bergman, L. Szunyogh, L. Nordström, and O. Eriksson, Phys. Rev. Lett. **111**, 127204 (2013).

[13] S. L. Dudarev, R. Bullough, and P. M. Derlet, Phys. Rev. Lett. **100**, 135503 (2008).

[14] M. Heine, O. Hellman, and D. Broido, Phys. Rev. B **100**, 104304 (2019).

[15] A. V. Ruban and O. E. Peil, Phys. Rev. B **97**, 174426 (2018).

[16] Z. Dong, W. Li, D. Chen, S. Schönecker, M. Long, and L. Vitos, Phys. Rev. B **95**, 054426 (2017).

[17] L. Mauger, M. S. Lucas, J. A. Muñoz, S. J. Tracy, M. Kresch, Y. Xiao, P. Chow, and B. Fultz, Phys. Rev. B **90**, 064303 (2014).

[18] J. Yin, M. Eisenbach, D. M. Nicholson, and A. Rusanu, Phys. Rev. B **86**, 214423 (2012).

[19] H. Wang, P.-W. Ma, and C. H. Woo, Phys. Rev. B **82**, 144304 (2010).

[20] J. Callaway and C. Wang, Physica B+C **91**, 337 (1977).

[21] J. Hubbard, Phys. Rev. B **19**, 2626 (1979).

[22] H. Hasegawa, J. Phys. Soc. Jpn. **46**, 1504 (1979).

[23] B. L. Gyorffy, A. J. Pindor, J. Staunton, G. M. Stocks, and H. Winter, J. Phys. F **15**, 1337 (1985).

[24] L. M. Small and V. Heine, J. Phys. F **14**, 3041 (1984).

[25] M. U. Luchini and V. Heine, Europhys. Lett. **14**, 609 (1991).

[26] O. Hellman, P. Steneteg, I. A. Abrikosov, and S. I. Simak, Phys. Rev. B **87**, 104111 (2013).

[27] O. Hellman and D. A. Broido, Phys. Rev. B **90**, 134309 (2014).

[28] O. Hellman, I. A. Abrikosov, and S. I. Simak, Phys. Rev. B **84**, 180301(R) (2011).

[29] A. H. Romero, E. K. U. Gross, M. J. Verstraete, and O. Hellman, Phys. Rev. B **91**, 214310 (2015).

[30] N. Metropolis and S. Ulam, J. Am. Stat. Assoc. **44**, 335 (1949).

[31] D. Frenkel and B. Smit, *Understanding Molecular Simulation: From Algorithms to Applications*, 2nd ed., Computational Science Series Vol. 1 (Academic, San Diego, 2002).

[32] D. P. Landau and K. K. Binder, *A Guide to Monte Carlo Simulations in Statistical Physics* (Cambridge University Press, Cambridge, U.K., 2015).

[33] N. Metropolis, A. Rosenbluth, M. Rosenbluth, A. Teller, and E. Teller, J. Chem. Phys. **21**, 1087 (1953).

[34] P.-W. Ma and S. L. Dudarev, Phys. Rev. B **91**, 054420 (2015).

[35] G. Kresse and J. Furthmüller, Comput. Mater. Sci. **6**, 15 (1996).

[36] G. Kresse and D. Joubert, Phys. Rev. B **59**, 1758 (1999).

[37] G. Kresse and J. Furthmüller, Phys. Rev. B **54**, 11169 (1996).

[38] G. Kresse and J. Hafner, Phys. Rev. B **48**, 13115 (1993).

[39] P. E. Blöchl, Phys. Rev. B **50**, 17953 (1994).

[40] D. Hobbs, G. Kresse, and J. Hafner, Phys. Rev. B **62**, 11556 (2000).

[41] J. P. Perdew, K. Burke, and M. Ernzerhof, Phys. Rev. Lett. **77**, 3865 (1996).

[42] Y. S. Touloukian, *Thermal Expansion: Thermophysical Properties of Matter*, Vol. 12 (Plenum, New York, 1975).

[43] See Supplemental Material at http://link.aps.org/supplemental/10.1103/PhysRevB.103.184409 for details on the artificial case studies, thermal expansion, and calculated phonon dispersions with comparison to measured data, which includes Refs. [7,14,18,35–42,44,51–55].

[44] J. Neuhaus, M. Leitner, K. Nicolaus, W. Petry, B. Hennion, and A. Hiess, Phys. Rev. B **89**, 184302 (2014).

[45] S. V. Halilov, H. Eschrig, A. Y. Perlov, and P. M. Oppeneer, Phys. Rev. B **58**, 293 (1998).

[46] I. Turek, J. Kudrnovský, V. Drchal, and P. Bruno, Philos. Mag. **86**, 1713 (2006).

[47] G. Shirane, V. J. Minkiewicz, and R. Nathans, J. Appl. Phys. **39**, 383 (1968).

[48] J. Neuhaus, W. Petry, and A. Krimmel, Physica B: Condens. Matter **234-236**, 897 (1997).

[49] O. Hellman and N. Shulumba, TDEP 1.1, https://ollehellman.github.io (2018).

[50] *MATLAB R2016b* (The MathWorks, Inc., Natick, MA, 2016).

[51] S. Klotz and M. Braden, Phys. Rev. Lett. **85**, 3209 (2000).

[52] V. J. Minkiewicz, G. Shirane, and R. Nathans, Phys. Rev. **162**, 528 (1967).

[53] F. Birch, Phys. Rev. **71**, 809 (1947).

[54] F. D. Murnaghan, Proc. Natl. Acad. Sci. USA **30**, 244 (1944).

[55] Z. S. Basinski, W. Hume-Rothery, and A. L. Sutton, Proc. R. Soc. London, Ser. A **229**, 459 (1955).